SETD2 suppresses tumorigenesis in a KRAS^{G12C}-driven lung cancer model and its catalytic activity is regulated by histone acetylation

Ricardo J. Mack[1,2,*], Natasha M. Flores[3,*], Geoffrey C. Fox[4], Hanyang Dong[1], Metehan Cebeci[1], Simone Hausmann[3], Tourkian Chasan[3], Jill M. Dowen[4,5,6,7,8], Brian D. Strahl[4,5,8], Pawel K. Mazur[3,#], and Or Gozani[1,2,#]

[1]Department of Biology, Stanford University, Stanford CA 94305 USA
[2]Cancer Biology Training Program, Stanford University, School of Medicine, Stanford CA 94305 USA
[3]Department of Experimental Radiation Oncology, The University of Texas MD Anderson Cancer Center, Houston, TX, 77030, USA
[4]Curriculum in Genetics & Molecular Biology, University of North Carolina at Chapel Hill, Chapel Hill, NC 27599, USA
[5]Department of Biochemistry & Biophysics, University of North Carolina at Chapel Hill, Chapel Hill, NC 27599, USA
[6]Department of Biology, University of North Carolina at Chapel Hill, Chapel Hill, NC 27599, USA
[7]Integrative Program for Biological and Genome Sciences, University of North Carolina at Chapel Hill, Chapel Hill, NC 27599, USA
[8]Lineberger Comprehensive Cancer Center, University of North Carolina at Chapel Hill, Chapel Hill, NC 27599, USA

[*]Equal contribution
[#]To whom correspondence should be addressed: pkmazur@mdanderson.org; ogozani@stanford.edu

Running title: Regulation of SETD2 methylation activity

ABSTRACT

Histone H3 trimethylation at lysine 36 (H3K36me3) is a key chromatin modification that regulates fundamental physiologic and pathologic processes. In humans, SETD2 is the only known enzyme that catalyzes H3K36me3 in somatic cells and is implicated in tumor suppression across multiple cancer types. While there is considerable crosstalk between the SETD2-H3K36me3 axis and other epigenetic modifications, much remains to be understood. Here, we show that SETD2 functions as a potent tumor suppressor in a $KRAS^{G12C}$-driven lung adenocarcinoma (LUAD) mouse model, and that acetylation at H3K27 (H3K27ac) enhances SETD2 *in vitro* methylation of H3K36 on nucleosome substrates. *In vivo*, *SETD2* ablation accelerates lethality in an autochthonous $KRAS^{G12C}$-driven LUAD mouse tumor model. Biochemical analyses reveal that polyacetylation of histone tails in a nucleosome context promote H3K36 methylation by SETD2. In addition, monoacetylation exerts position-specific effects to stimulate SETD2 methylation activity. In contrast, mono-ubiquitination at various histone sites, including at H2AK119 and H2BK120, does not affect SETD2 methylation of nucleosomes. Together, these findings provide insight into how SETD2 integrates histone modification signals to regulate H3K36 methylation and highlights the potential role of SETD2-associated epigenetic crosstalk in cancer pathogenesis.

INTRODUCTION

Protein lysine methylation is a common post-translational modification (PTM) that occurs in three distinct states—monomethylation (Kme1), dimethylation (Kme2), and trimethylation (Kme3)—depending on whether one, two or three methyl groups are added to the lysine sidechain (1). Lysine methylation is catalyzed by a class of enzymes named protein lysine methyltransferases (KMTs) and removed by protein lysine demethylases (1). Methylation at H3K36 is an evolutionarily conserved histone modification (2). In humans, mutations in the enzymes that determine H3K36 methylation dynamics are linked to a variety of developmental disorders and cancer (2-4). The state and extent of methylation at H3K36 is synthesized by distinct KMTs, with H3K36me2 generated by four related enzymes (NSD1, NSD2, NSD3, and ASH1L), whereas SETD2 is the only human enzyme in somatic cells that has been reproducibly shown to generate H3K36me3 (2, 3, 5). SETD2 and its cognate mark H3K36me3 generally occupy transcriptionally active regions. Functionally, SETD2 influences core molecular processes such as DNA methylation, RNA processing, DNA repair, and genomic integrity (6-11). Notably, while H3K36me2-generating enzymes like NSD2 and NSD3 promote oncogenesis when mutated or overexpressed (e.g. (12-17)), SETD2 is a potent tumor suppressor frequently mutated in clear cell renal cell carcinoma (ccRCC) (9, 18) and several other cancers. For example, the *SETD2* gene (along with other important tumor suppressors) is located within chromosome 3p, a genomic region that is reported to show loss of heterozygosity in ~90-95% of ccRCC tumors (19). In ccRCC pathogenesis, ~10-20% of tumors acquire SETD2 mutation on the second intact allele (or more rarely acquire mutations on both alleles) resulting in biallelic loss of *SETD2* and H3K36me3 depletion (9, 18, 19). Deletions and/or loss-of-function mutations in SETD2 are also detected

recurrently in different types of leukemia and solid tumors including gastroesophageal cancers and lung adenocarcinoma (LUAD), though at lower frequency than seen in ccRCC (10, 20-23).

SETD2 is a large protein with multiple functional regions and domains beyond its ability to catalyze H3K36me3. Thus, the precise role of H3K36me3 in SETD2-associated functions remain unclear. One established function of SETD2-catalyzed H3K36me3 is to allosterically inhibit the ability of the PRC2 complex to synthesize the repressive H3K27me3 chromatin modification (24-29). Further, H3K36me3, via its recognition by the PWWP domain of DNMT3b, promotes targeted DNA methylation (6). However, beyond H3K27me3 and DNA methylation, potential crosstalk between other epigenetic modifications and SETD2-mediated catalysis of H3K36me3 in the regulation of SETD2 function are relatively unexplored. Here, we test the *in vivo* role of SETD2 in suppressing $KRAS^{G12C}$-driven tumorigenesis in LUAD, as G12C is the most common KRAS mutation in this tumor type, and identify potential regulatory roles for histone acetylation, particularly H3K27 acetylation, in promoting *in vitro* methylation of nucleosomes by SETD2.

RESULTS

SETD2 deletion accelerates $KRAS^{G12C}$-driven lung cancer pathogenesis in vivo

Several elegant previous *in vivo* studies utilizing either CRISPR-based or gene knockout approaches demonstrated that loss of SETD2 promotes lung adenocarcinoma (LUAD) tumorigenesis in the canonical $KRAS^{G12D}$-driven LUAD mouse tumor model (22, 30-33). As G12C is the most common KRAS oncogenic variant in LUAD (34, 35), we used a recently developed $KRAS^{G12C}$-driven LUAD mouse model (named K^cP) (36) to test whether the additional loss of SETD2 (named $K^cP;Setd2$) impacted cancer pathogenesis *in vivo* like it does in a G12D oncogenic mutant background (Figs. 1A-C). In this model, expression of the $Kras^{G12C}$ mutant allele

and homozygous deletions of *p53* and *Setd2* are induced by intratracheal lavage of adenovirus expressing Cre recombinase (Ad-Cre) (36). Following viral infection, *K^{c}P* mutant mice develop widespread LUAD with 100% penetrance (see schematic, Fig. 1D; (36)). Consistent with the principal catalytic activity of SETD2 being generation of H3K36me3, *SETD2* deletion resulted in loss of H3K36me3 immunohistochemistry (IHC) signal comparing LUAD tissue sections from *K^{c}P* and *K^{c}P;Setd2* mice (Fig. 1E). Moreover, *SETD2* depletion accelerated tumorigenesis as measured by a modest increase in tumor nodule numbers and a four-fold increase in tumor burden (Figs. 1F-G). Loss of SETD2 also caused an increase in cellular proliferation in tumors, but did not significantly impact apoptosis levels (Figs. 1E, H-I). Finally, SETD2 depletion resulted in a 40% decline in animal overall median survival time (Fig. 1J). Thus, as previously observed with oncogenic KRAS^{G12D}-based models (22, 30-33), SETD2 loss accelerates mutant KRAS^{G12C}-driven malignancy *in vivo*.

SETD2 in vitro methylation activity on H3K36 methylated nucleosomes

In humans, SETD2 is the only enzyme in somatic cells that generates the canonical epigenetic modification H3K36me3 (5). In contrast, four KMTs (NSD1, NSD2, NSD3, and ASH1L) generate H3K36me2 (3). Notably, while SETD2 is tumor suppressive (e.g. see Fig. 1), the H3K36me2 KMTs are generally oncogenic (3). While the specific role of SETD2-catalyzed H3K36me3 in cancer pathogenesis remains unclear, it is intriguing that the di-methyl and tri-methyl states at H3K36 may have profoundly different impacts on tumorigenesis. In this regard, it has been postulated that SETD2 requires pre-existing H3K36me2 to generate the tri-methyl state at K36 (2, 3). However, previous work demonstrated that the isolated catalytic SET domain of SETD2 methylates unmodified recombinant Nucleosomes (rNucs) *in vitro* with the same efficiency as

methyl-lysine analog (MLA)-based H3K$_C$36me2 rNucs (37). While MLA chemistry is generally able to faithfully model native methyl-lysine function (e.g., recognition by reader domains), there are examples where the sulfur moiety compromises functionality (38). Thus, we tested the impact of native methylation installed at H3K36 on the enzymatic activity of the catalytic region of SETD2 that encompasses the SET domain as well as the pre- and post-SET regions (hereafter named SETD2$_{SET}$; Fig. 2A).

In vitro methylation assays were performed using recombinant SETD2$_{SET}$, radiolabeled *S*-Adenosyl-methionine (SAM) as the methyl donor, and rNucs that were either unmethylated or harboring me1, me2, or me3 at K36 as substrate. The SETD2$_{SET}$ domain methylated all the rNuc substrates besides the tri-methylated sample (Fig. 2B). Specifically, the highest signal was observed using unmodified rNucs, with the intensity of the signal decreasing sequentially on H3K36me1 and H3K36me2 rNuc substrates, likely reflecting the reduced capacity of these H3K36 methylated histones to be further methylated (Fig. 2B). SETD2$_{SET}$ showed no detectable methylation activity on H3K36me3 rNucs, consistent with K36 being 100% saturated with methylation and thus there being no more sites available to be methylated and the specificity of SETD2 for K36 versus other lysine residues on histones (Fig. 2B). Similar results were observed using an independent quantitative method that measures production of *S*-Adenosyl-homocysteine (SAH) – a key byproduct of the methylation reaction (Fig. 2C). Like with SETD2$_{SET}$, the NSD2$_{SET}$ domain showed the strongest methylation activity on unmodified rNucs compared to H3K36me1 rNucs, and NSD2$_{SET}$ has no activity on H3K36me2/3 rNucs, consistent with NSD2 being a selective H3K36me2-KMT (Fig. 2D).

To gain insight into the efficiency of conversion between methyl states at K36 for SETD2, we identified methyl-state specific H3K36 antibodies for the three methyl states (Fig. 2E). We next

tested how lysine methyl-state transition on the various H3K36 methylated nucleosome substrates impact $SETD2_{SET}$ activity. To this end, we performed methylation assays with $SETD2_{SET}$ using non-radiolabeled SAM and detected modification of rNucs using the H3K36me state-specific antibodies (Fig. 2E). Under our reaction conditions (see Methods), $SETD2_{SET}$ generated all three methyl states (me1, me2, and me3) when using unmodified rNucs as substrate (Fig. 2F). On H3K36me1-rNucs, $SETD2_{SET}$ generated both higher states of methylation at K36 (H3K36me2 and H3K36me3), whereas H3K36me2-rNucs were naturally only converted to the trimethyl state (Fig. 2F). The conversion to the trimethyl state at K36 was most efficient on H3K36me2-rNucs, which likely reflects the reaction having poor *in vitro* processivity (Fig. 2F). These results indicate that the ability of $SETD2_{SET}$ to generate H3K36me3 *in vitro* does not require pre-existing methylation, consistent with previous studies (37). The data further suggests that, at least *in vitro*, $SETD2_{SET}$ is agnostic about the state of methylation at H3K36 on nucleosome substrates.

Specific histone acetylation events enhance SETD2 methylation activity

Histone acetylation promotes transcription and other DNA-templated processes through several mechanisms, such as the recognition of acetyl-lysine by reader proteins and the neutralization of DNA-histone interactions (39-41). The combined consequences of such activities decondense chromatin to increase accessibility to the underlying DNA. In addition, neutralizing the positive charge on the lysine side chain facilitates accessibility of KMTs to the unstructured histone tails by disrupting tail-DNA interactions, as was previously shown for the MLL1 KMT complex (40-43). Given the relatively restrictive location of K36 of H3 near the globular domain of the nucleosome, we speculated that histone acetylation might render the residue more accessible to methylation by SETD2. To test this idea, methylation assays with $SETD2_{SET}$ were performed

using substrates that were either unmodified rNucs or rNucs with tetra-acetylated lysine residues on the N-terminus tails of H2A, H3, or H4 (see schematic, Fig. 3A). $SETD2_{SET}$ methylation activity as determined by incorporation of radiolabeled SAM or SAH production was enhanced on tetra-acetylated rNucs compared to control rNucs irrespective of the acetylated histone tail (Figs. 3B-C). A similar trend was observed in methylation assays using the $NSD2_{SET}$ domain, though H3 tetra-acetylation seemed to have the biggest impact compared to acetylation of H2A and H4 (Fig. 3D). In contrast, methylation assays using hDOT1L, the KMT responsible for H3K79 methylation – a PTM situated in the nucleosome globular domain – was not enhanced by acetylation of the various histone tails (Fig. 3E). Collectively, these data suggest that a high degree of acetylation may increase the accessibility of H3K36 to the enzymes that methylate this residue.

We next explored whether acetylation of individual residues on the H3 tail could facilitate SETD2 activity, and if so, whether such an effect depends on the specific acetylation site. To this end, methylation assays with $SETD2_{SET}$ were performed using substrates that were either unmodified rNucs or rNucs mono-acetylated at K4, K9, K14, K18, K23, or K27 on the N-terminal tail of H3 (see schematic, Fig. 4A). Methylation activity, determined by incorporation of radiolabeled SAM (Fig. 4B) or SAH production (Fig. 4C), indicated that three different single acetylation sites (K14, K23, and K27) enhanced $SETD2_{SET}$ methylation activity on nucleosomes, with the impact likely H3K27ac>H3K14ac>H3K23ac (Figs. 4B-C). While understanding the molecular basis for the acetylation-mediated enhancement in SETD2 activity will likely require structural investigation, we reasoned that given the proximity and relationship between H3K27 and H3K36 (24, 44), that acetylation at K27 might impact the interaction between $SETD2_{SET}$ and nucleosomes. Intriguingly, the ability of $SETD2_{SET}$ to form a complex with recombinant mono-nucleosomes was slightly enhanced in the presence of K27 acetylation (Fig. 4D). Consistent with

this, $SETD2_{SET}$ was more efficiently pulled down when using H3K27ac rNucs as bait compared to unmodified rNucs (Fig. 4E), suggesting that there may be a potential role for K27ac in contributing to the interaction between $SETD2_{SET}$ and its substrate site in the context of nucleosomes (see Discussion).

Histone ubiquitination does not impact SETD2 methylation activity in vitro

We next investigated how ubiquitination at various histone residues influences SETD2 activity. While methylation at H3K36 directly blocks a key allosteric interaction between the PRC2 complex and unmodified H3K36, H3K27me3 indirectly inhibits H3K36 KMTs. Specifically, H3K27me3 recruits the PRC1 complex, which catalyzes the ubiquitination of H2AK119 (H2AK119ub) (45). Nucleosomes harboring H2AK119ub antagonize H3K36 enzymes like NSD2 by structurally preventing their proper association with the nucleosome (44). However, whether H2AK119ub and/or other histone ubiquitination sites impact SETD2 activity is unclear, although studies in yeast have shown the SETD2 homolog, Set2, is influenced by H2BK120ub (46). Thus, we tested $SETD2_{SET}$ activity against a library of ubiquitinated nucleosomes as substrates (see schematic, Fig. 5A). Surprisingly, assaying methylation by three different methods (utilizing radiolabeled SAM, detecting the different methylation states by Western, and measuring SAH generation), histone ubiquitination did not impact SETD2 activity (Fig. 5B-D; note that the H3K36me2 antibody is blocked by H3K14 and H3K18 ubiquitination). In contrast, as expected, H2AK119ub specifically reduced NSD2 activity (Fig. 5E). Collectively, these findings indicate that the isolated catalytic domain of SETD2, unlike for NSD2, is not influenced by histone ubiquitination, suggesting potential functional differences in how H3K36 enzymes interact with the ubiquitinated nucleosome landscape.

DISCUSSION

SETD2, via catalytic and non-catalytic mechanisms, regulates fundamental nuclear processes. Mutations in SETD2 cause Sotos-like syndrome, an overgrowth disorder, and loss of SETD2 commonly occurs and is thought to be tumor suppressive in ccRCC and many other malignancies (3, 47). Indeed, SETD2 was identified as one of the most mutated genes in a saturation analysis of 21 cancer types (48). Consistent with these observations and previous lung cancer mouse modeling studies (22, 32, 33), we find that SETD2 ablation strongly accelerates LUAD malignant progression and lethality in a $KRAS^{G12C}$-driven mouse tumor model (see Fig. 1). While these studies demonstrate that CRISPR-mediated endogenous depletion of SETD2 or homozygous genetic deletion of *SETD2* promote tumorigenesis, future work will help elucidate the specific contributions of H3K36me3 synthesis and other SETD2 functional domains in tumor suppression. In this context, EZM0414, a clinical-grade SETD2 inhibitor, was being evaluated in a Phase I clinical trial as a therapeutic in relapsed or refractory multiple myeloma and diffuse large B cell lymphoma, suggesting that at least in these cancer types, H3K36me3 generation may be oncogenic (NCT05121103; note this trial was terminated). Whether SETD2-mediated catalysis of H3K36me3 is tumor suppressive or oncogenic in a tumor context-dependent manner—and how this activity relates to SETD2's other functions—are potentially important questions for future investigation.

Consistent with previous work, our biochemical analyses using native designer nucleosomes indicates that—at least in isolation—the catalytic domain of SETD2 does not exhibit a preference for substrates bearing mono- or di-methylation at K36 compared to the unmodified state (see Fig. 2) (37). We speculate that physiologically SETD2 uses all three lower states of methylation at

H3K36me (me0-me2) to generate endogenous H3K36me3, with the specific precursor state determined by the underlying biology and genomic context. Our analyses also uncovered an unanticipated regulatory role for histone acetylation in activating SETD2 *in vitro* methylation activity on nucleosomes. Why some acetylation sites increased SETD2 activity whereas others did not is presently unclear. One possibility is that certain acetylation events, for example H3K27ac, may alter histone-DNA interactions in a manner that renders H3K36 more accessible to the catalytic pocket of SETD2. Additionally, our data suggests that SETD2 may interact more strongly with H3K27ac nucleosomes compared to unmodified nucleosomes, which would promote higher levels of methylation (Fig. 4). Finally, we observed a divergence between SETD2 and H3K36me2-KMTs such as NSD2, in that SETD2 is neither inhibited by H2AK119ub nor regulated by H2BK120ub (Fig. 5). These data are consistent with recent cryo-EM-based structural studies, which provide a molecular rationale for why NSD2, but not SETD2, would be impacted by a large modification within the C-terminal region of H2A (44, 49, 50). Future functional and epigenomic studies will be crucial for understanding how epigenetic modifications such as acetylation and ubiquitination regulate SETD2 activity in physiological and pathological settings.

MATERIALS & METHODS

Protein expression and purification

The $SETD2_{SET}$ (aa1418-1714, NCBI Sequence: NC_000003.12), $NSD2_{SET}$ (aa959-1365, NCBI Sequence: NC_000004.12), and DOT1L (aa1-416, NCBI Sequence: NC_000019.10) were cloned into pGEX-6P-1 separately. *Escherichia coli* Rossetta cells were transformed with the respective expression vectors and cultured in LB medium (10 g/L tryptone, 5 g/L yeast extract, and 10 g/L NaCl) supplemented with 0.1 mM IPTG (isopropyl 1-thio-β-D-galactopyranoside, Sigma) at 18 °C for 16–20 h. Cells were lysed using sonicator, lysates were cleared by centrifugation at 12,000 rpm for 20 min and the supernatants were incubated with Glutathione Sepharose (GE Healthcare); bound proteins were washed and eluted in 10 mM reduced glutathione (Sigma). Protein concentrations were measured using Pierce Coomassie Plus Assay.

For expression and purification of GST-SETD2 (1345-1711) used in Figure 4D, BL21.DE3(pLysS) E. coli transformed with a recombinant expression plasmid encoding GST-tagged human SETD2 catalytic domain (residues 1345-1711) was grown in LB supplemented with 50 µg/mL carbenicillin at 37° C until OD600 reached ~0.6. Cultures were then transferred to 16° C and induced with 1 mM IPTG (Sigma) overnight and harvested by centrifugation, flash frozen in liquid nitrogen, and stored at -20° C until use. Thawed cell pellets were resuspended in lysis buffer (50 mM HEPES pH 7.5, 150 mM NaCl, 1 mM DTT, 1 mM PMSF) supplemented with 250 U of Pierce Universal Nuclease (ThermoFisher) and 1 mg/mL lysozyme (Sigma) and incubated at 37° C for 10 minutes. Cells were then lysed by sonication (5 x 30 seconds, 40% cycle, 40% power) and lysates clarified by centrifugation before application to glutathione agarose beads (Pierce) pre-equilibrated in wash buffer (50 mM HEPES pH 7.5, 150 mM NaCl, 1 mM DTT, 1 mM PMSF). Following three sequential washes with wash buffer, proteins were eluted in ~1 mL fractions with

wash buffer supplemented with 10 mM glutathione. Fractions containing purified GST-SETD2 were pooled, concentrated by centrifugation filtration (EMD Millipore, MWCO 30 kDa). Glycerol was added to 20% final concentration, aliquoted, and stored at -80°C until use (51).

In vitro methylation reactions

The methylation reactions on nucleosomes were performed similar as previously described (52). Briefly, 350 nM recombinant enzymes were mixed with 500 nM mononucleosome (EpiCypher) in reaction buffer (containing 250 mM Tris pH 8.0, 100 mM KCl, 25 mM $MgCl_2$ and 50% glycerol), after adding 20 μM SAM (S-adenosylmethionine), the mixture was incubated at 30°C for 3 hours.

MTase-Glo methyltransferase assay

The MTase-Glo methyltransferase assay kit (Promega) was used to measure enzymatic activity in the presence of different substrates. Specifically, we established an assay in 10 μL reaction mix containing 35 nM of KMT enzyme, 4 μM SAM, 50 nM mononucleosomes (EpiCypher), and MTase-Glo reagent (1×) in reaction buffer (containing 250 mM Tris pH 8.0, 100 mM KCl, 25 mM MgCl2 and 50% glycerol) arrayed in a white 384-well microplate (Corning). Each independent biochemical reaction was performed in triplicate and incubated for 3 hours at 30°C. Subsequently, 10 μL of MTase-Glo detection solution was added and incubated for 1 hour at room temperature. Reactions were detected by luminescence.

Western blot analyses

For western blot analysis, protein samples were resolved by SDS–PAGE and transferred to a PVDF membrane. The following antibodies were used (at the indicated dilutions): H3K36me1 (Abclonal #A11141, 1:1000), H3K36me2 (ThermoFisher #701767, 1:1000), H3K36me3 (EpiCypher #13-0058, 1:1,000), H3 (EpiCypher #13-0001, 1:10000).

Animal models

Kras$^{cKI\text{-}G12C}$ and *Trp53*$^{loxP/loxP}$ mutant mice have been described before (36, 53). Conditional *Setd2*$^{loxP/loxP}$ mouse strain was obtained from Shanghai Model Organisms Center, Inc (Cat. NO. NM-CKO-190069). Briefly, the Setd2$^{loxP/loxP}$ targeted knockin sequence includes the Neo-LacZ cassette flanked by Frt sites and exon 3 sequence flanked by LoxP sites. Founder mice were crossed with Rosa26-FlpO deleter strain (54) to generate *Setd2*$^{loxP/loxP}$ conditional allele. Confirmation of *Setd2*$^{loxP/loxP}$ conditional allele targeting was performed by PCR on DNA isolated from mouse tail biopsies and the following primers: Forward: AGCTGACCTGATTTCTCCTTTAG; Reverse: AACAGCTGAGAGTGACCATGAG. Mice were maintained on a mixed C57BL/6;FVB strain background and we systematically used littermates as controls in all the experiments. Both male and female animals were used in the experiments, and no sex differences were noted. In all experiments, animals were numbered, and experiments were conducted in a blinded fashion. After data collection, genotypes were revealed, and animals were assigned to groups for analysis. None of the mice with the appropriate genotype were excluded from this study or used in any other experiments. All mice were co-housed with littermates (2–5 per cage) in pathogen-free facility with standard controlled temperature of 72 °F, with a humidity of 30–70%, and a light cycle of 12 h on/12 h off set from 7am to 7pm and with unrestricted access to standard food and water under the supervision of veterinarians, in an

AALAC-accredited animal facility at the University of Texas M.D. Anderson Cancer Center (MDACC). Mouse handling and care followed the NIH Guide for Care and Use of Laboratory Animals. All animal procedures followed the guidelines of and were approved by the MDACC Institutional Animal Care and Use Committee (IACUC protocol 00001636, PI: Mazur).

To evaluate the effects of SETD2 ablation on the development and progression of lung adenocarcinoma, we utilized *Kras*$^{cKI\text{-}G12C/+}$, *Trp53*$^{loxP/loxP}$ (*K*^{C}*P*), and *Kras*$^{cKI\text{-}G12C/+}$, *Trp53*$^{loxP/loxP}$, *Setd2*$^{loxP/loxP}$ (*K*^{C}*P;Setd2*). To generate tumors in the lungs of *K*^{C}*P;Setd2* and control *K*^{C}*P* mutant mice we used replication-deficient adenoviruses expressing Cre-recombinase (Ad-Cre) as previously described (55). Briefly, 8-week-old mice were anesthetized by continuous gaseous infusion of 2% isoflurane for at least 10 min using a veterinary anesthesia system. Ad-Cre was delivered to the lungs by intratracheal lavage. Prior to administration, the virus was precipitated with calcium phosphate to improve the delivery of Cre by increasing the efficiency of viral infection of the lung epithelium. Mice were treated with one dose of 5×10^6 PFU of Ad-Cre. Mice were analyzed for tumor formation and progression at indicated timepoints after viral infection. The survival endpoint was determined by overall health criteria scoring. Mouse health status and weight were checked daily.

Histology and immunohistochemistry

Tissue specimens were fixed in 4% buffered formalin for 24 hours and stored in 70% ethanol until paraffin embedding. 3-µm sections were stained with hematoxylin and eosin (HE) or used for immunostaining studies. The following antibodies were used (at the indicated dilutions): cleaved Caspase 3 (CST #9664, 1:200), Ki67 (BD Bioscience #550609, 1:1000), H3K36me3 (CST #4909, 1:1000). Immunohistochemistry (IHC) was performed on formalin-fixed, paraffin-

embedded tissue (FFPE) sections using a biotin-avidin HRP conjugate method (Vectastain ABC-HRP kit, #PK4000) as described before (56). Sections were developed with DAB and counterstained with hematoxylin. Pictures were taken using a PreciPoint M8 microscope equipped with the PointView software and quantified using Image J software (v1.53k, RRID:SCR_003070) and QuPath (v0.5.1, RRID:SCR_018257).

Nucleosome pulldown assays

2.5 pmol of GST-SETD2 was added to nucleosome binding buffer (50 mM Tris-Cl pH 7.6, 300 mM NaCl, 0.1% NP-40, 0.5% bovine serum albumin, 10% glycerol) to a final volume of 25 µL. 12.5 pmol of biotinylated nucleosome was added and rotated overnight at 4° C. 1 µL of streptavidin Dynabeads (Fisher) were equilibrated in nucleosome binding buffer and resuspended to a final volume of 7.5 µL. Resuspended beads were then added to the nucleosome-enzyme mixture and rotated at 4° C for 1 hour. Beads were pelleted on a magnet, the supernatant (unbound) fraction was collected, and the beads were washed with 200 µL of nucleosome binding buffer three times. Following the final wash, beads were resuspended in 15 µL of a 1x SDS-PAGE loading dye and stored at 4° C until immunoblotting.

Electromobility shift assay (EMSA)

Nucleosomes were incubated with recombinant $SETD2_{SET}$ in EMSA buffer (30 mM Tris-HCl pH 7.5, 100 mM KCl, 25 mM $MgCl_2$, 6 mM DTT (Dithiothreitol), 0.0075% Tween 20, 12% Glycerol) for 15 min at room temperature and analyzed by native 0.2X TBE-PAGE. Each reaction contained 250 nM of nucleosome with increasing concentrations of domain (0, 1, 2, 3, 4, 5 µM). Gels were stained with Sybr Gold.

Quantification and statistical analysis

Please refer to the Figure legends or the Experimental Details for description of sample size (n) and statistical details. All values for n are for individual mice or individual samples. Sample sizes were chosen based on previous experience with given experiments. Differences were statistically analyzed by unpaired two-tailed t-test, and one-way ANOVA with Dunnet's test for multiple comparisons as indicated.

Acknowledgements

This work was supported in part by grants from the NIH to O.G. (R35 GM139569), O.G. and P.K.M. (R01 CA272844, R01 CA278940), P.K.M. (R01 CA236949, R01 CA266280, R01 CA272843). P.K.M. is also supported by DoD PRCRP Career Development Award (CA181486), CPRIT IIRA (RP220391) and CPRIT Scholar in Cancer Research (RR160078). R.M. is supported by a DARE fellowship. This work was also supported in part by grants from the NIH to B.D.S. (R35 GM126900) and J.M.D. (R35 GM152103). G.C.F. was supported by a predoctoral training grant from the National Institute for General Medical Sciences (T32 GM135128).

REFERENCES:

1. Bhat, K. P., Umit Kaniskan, H., Jin, J., and Gozani, O. (2021) Epigenetics and beyond: targeting writers of protein lysine methylation to treat disease *Nat Rev Drug Discov* 10.1038/s41573-020-00108-x
2. Li, J., Ahn, J. H., and Wang, G. G. (2019) Understanding histone H3 lysine 36 methylation and its deregulation in disease *Cell Mol Life Sci* **76**, 2899-2916 10.1007/s00018-019-03144-y
3. Husmann, D., and Gozani, O. (2019) Histone lysine methyltransferases in biology and disease *Nat Struct Mol Biol* **26**, 880-889 10.1038/s41594-019-0298-7
4. Bennett, R. L., Swaroop, A., Troche, C., and Licht, J. D. (2017) The Role of Nuclear Receptor-Binding SET Domain Family Histone Lysine Methyltransferases in Cancer *Cold Spring Harb Perspect Med* **7**, 10.1101/cshperspect.a026708
5. Edmunds, J. W., Mahadevan, L. C., and Clayton, A. L. (2008) Dynamic histone H3 methylation during gene induction: HYPB/Setd2 mediates all H3K36 trimethylation *EMBO J* **27**, 406-420 7601967 [pii]10.1038/sj.emboj.7601967
6. Baubec, T., Colombo, D. F., Wirbelauer, C., Schmidt, J., Burger, L., Krebs, A. R. *et al.* (2015) Genomic profiling of DNA methyltransferases reveals a role for DNMT3B in genic methylation *Nature* **520**, 243-247 10.1038/nature14176
7. Jha, D. K., Pfister, S. X., Humphrey, T. C., and Strahl, B. D. (2014) SET-ting the stage for DNA repair *Nat Struct Mol Biol* **21**, 655-657 10.1038/nsmb.2866
8. de Almeida, S. F., Grosso, A. R., Koch, F., Fenouil, R., Carvalho, S., Andrade, J. *et al.* (2011) Splicing enhances recruitment of methyltransferase HYPB/Setd2 and methylation of histone H3 Lys36 *Nat Struct Mol Biol* **18**, 977-983 10.1038/nsmb.2123
9. Duns, G., van den Berg, E., van Duivenbode, I., Osinga, J., Hollema, H., Hofstra, R. M. *et al.* (2010) Histone methyltransferase gene SETD2 is a novel tumor suppressor gene in clear cell renal cell carcinoma *Cancer Res* **70**, 4287-4291 0008-5472.CAN-10-0120 [pii]10.1158/0008-5472.CAN-10-0120
10. Zhu, X., He, F., Zeng, H., Ling, S., Chen, A., Wang, Y. *et al.* (2014) Identification of functional cooperative mutations of SETD2 in human acute leukemia *Nature Genetics* **46**, 287-293 10.1038/ng.2894
11. Wen, H., Li, Y., Xi, Y., Jiang, S., Stratton, S., Peng, D. *et al.* (2014) ZMYND11 links histone H3.3K36me3 to transcription elongation and tumour suppression *Nature* **508**, 263-268 10.1038/nature13045
12. Kuo, A. J., Cheung, P., Chen, K., Zee, B. M., Kioi, M., Lauring, J. *et al.* (2011) NSD2 Links Dimethylation of Histone H3 at Lysine 36 to Oncogenic Programming *Mol Cell* **44**, 609-620 S1097-2765(11)00813-6 [pii]10.1016/j.molcel.2011.08.042
13. Hudlebusch, H. R., Santoni-Rugiu, E., Simon, R., Ralfkiaer, E., Rossing, H. H., Johansen, J. V. *et al.* (2011) The histone methyltransferase and putative oncoprotein MMSET is overexpressed in a large variety of human tumors *Clin Cancer Res* **17**, 2919-2933 10.1158/1078-0432.CCR-10-1302
14. Jaffe, J. D., Wang, Y., Chan, H. M., Zhang, J., Huether, R., Kryukov, G. V. *et al.* (2013) Global chromatin profiling reveals NSD2 mutations in pediatric acute lymphoblastic leukemia *Nat Genet* **45**, 1386-1391 10.1038/ng.2777

15. Aytes, A., Giacobbe, A., Mitrofanova, A., Ruggero, K., Cyrta, J., Arriaga, J. *et al.* (2018) NSD2 is a conserved driver of metastatic prostate cancer progression *Nat Commun* **9**, 5201 10.1038/s41467-018-07511-4
16. Yuan, G., Flores, N. M., Hausmann, S., Lofgren, S. M., Kharchenko, V., Angulo-Ibanez, M. *et al.* (2021) Elevated NSD3 histone methylation activity drives squamous cell lung cancer *Nature* **590**, 504-508 10.1038/s41586-020-03170-y
17. Sengupta, D., Zeng, L., Li, Y., Hausmann, S., Ghosh, D., Yuan, G. *et al.* (2021) NSD2 dimethylation at H3K36 promotes lung adenocarcinoma pathogenesis *Mol Cell* **81**, 4481-4492 e4489 10.1016/j.molcel.2021.08.034
18. Dalgliesh, G. L., Furge, K., Greenman, C., Chen, L., Bignell, G., Butler, A. *et al.* (2010) Systematic sequencing of renal carcinoma reveals inactivation of histone modifying genes *Nature* **463**, 360-363 nature08672 [pii]10.1038/nature08672
19. Walton, J., Lawson, K., Prinos, P., Finelli, A., Arrowsmith, C., and Ailles, L. (2023) PBRM1, SETD2 and BAP1 - the trinity of 3p in clear cell renal cell carcinoma *Nat Rev Urol* **20**, 96-115 10.1038/s41585-022-00659-1
20. Foggetti, G., Li, C., Cai, H., Hellyer, J. A., Lin, W. Y., Ayeni, D. *et al.* (2021) Genetic Determinants of EGFR-Driven Lung Cancer Growth and Therapeutic Response In Vivo *Cancer Discov* **11**, 1736-1753 10.1158/2159-8290.CD-20-1385
21. Kadara, H., Choi, M., Zhang, J., Parra, E. R., Rodriguez-Canales, J., Gaffney, S. G. *et al.* (2017) Whole-exome sequencing and immune profiling of early-stage lung adenocarcinoma with fully annotated clinical follow-up *Ann Oncol* **28**, 75-82 10.1093/annonc/mdw436
22. Walter, D. M., Venancio, O. S., Buza, E. L., Tobias, J. W., Deshpande, C., Gudiel, A. A. *et al.* (2017) Systematic In Vivo Inactivation of Chromatin-Regulating Enzymes Identifies Setd2 as a Potent Tumor Suppressor in Lung Adenocarcinoma *Cancer Res* **77**, 1719-1729 10.1158/0008-5472.CAN-16-2159
23. Mar, B. G., Chu, S. H., Kahn, J. D., Krivtsov, A. V., Koche, R., Castellano, C. A. *et al.* (2017) SETD2 alterations impair DNA damage recognition and lead to resistance to chemotherapy in leukemia *Blood* **130**, 2631-2641 10.1182/blood-2017-03-775569
24. Cookis, T., Lydecker, A., Sauer, P., Kasinath, V., and Nogales, E. (2025) Structural basis for the inhibition of PRC2 by active transcription histone posttranslational modifications *Nat Struct Mol Biol* **32**, 393-404 10.1038/s41594-024-01452-x
25. Yuan, W., Xu, M., Huang, C., Liu, N., Chen, S., and Zhu, B. (2011) H3K36 methylation antagonizes PRC2-mediated H3K27 methylation *J Biol Chem* **286**, 7983-7989 10.1074/jbc.M110.194027
26. Schmitges, F. W., Prusty, A. B., Faty, M., Stutzer, A., Lingaraju, G. M., Aiwazian, J. *et al.* (2011) Histone methylation by PRC2 is inhibited by active chromatin marks *Mol Cell* **42**, 330-341 10.1016/j.molcel.2011.03.025
27. Jani, K. S., Jain, S. U., Ge, E. J., Diehl, K. L., Lundgren, S. M., Muller, M. M. *et al.* (2019) Histone H3 tail binds a unique sensing pocket in EZH2 to activate the PRC2 methyltransferase *Proc Natl Acad Sci U S A* **116**, 8295-8300 10.1073/pnas.1819029116
28. Finogenova, K., Bonnet, J., Poepsel, S., Schafer, I. B., Finkl, K., Schmid, K. *et al.* (2020) Structural basis for PRC2 decoding of active histone methylation marks H3K36me2/3 *Elife* **9**, 10.7554/eLife.61964
29. Chen, H., Hu, B., Horth, C., Bareke, E., Rosenbaum, P., Kwon, S. Y. *et al.* (2022) H3K36 dimethylation shapes the epigenetic interaction landscape by directing repressive

chromatin modifications in embryonic stem cells *Genome Res* **32**, 825-837 10.1101/gr.276383.121
30. Johnson, L., Mercer, K., Greenbaum, D., Bronson, R. T., Crowley, D., Tuveson, D. A. *et al.* (2001) Somatic activation of the K-ras oncogene causes early onset lung cancer in mice *Nature* **410**, 1111-1116 10.1038/35074129
31. Jackson, E. L., Willis, N., Mercer, K., Bronson, R. T., Crowley, D., Montoya, R. *et al.* (2001) Analysis of lung tumor initiation and progression using conditional expression of oncogenic K-ras *Genes Dev* **15**, 3243-3248 10.1101/gad.943001
32. Rogers, Z. N., McFarland, C. D., Winters, I. P., Seoane, J. A., Brady, J. J., Yoon, S. *et al.* (2018) Mapping the in vivo fitness landscape of lung adenocarcinoma tumor suppression in mice *Nat Genet* **50**, 483-486 10.1038/s41588-018-0083-2
33. Xie, Y., Sahin, M., Wakamatsu, T., Inoue-Yamauchi, A., Zhao, W., Han, S. *et al.* (2023) SETD2 regulates chromatin accessibility and transcription to suppress lung tumorigenesis *JCI Insight* **8**, 10.1172/jci.insight.154120
34. Campbell, J. D., Alexandrov, A., Kim, J., Wala, J., Berger, A. H., Pedamallu, C. S. *et al.* (2016) Distinct patterns of somatic genome alterations in lung adenocarcinomas and squamous cell carcinomas *Nat Genet* **48**, 607-616 10.1038/ng.3564
35. Wiesweg, M., Kasper, S., Worm, K., Herold, T., Reis, H., Sara, L. *et al.* (2019) Impact of RAS mutation subtype on clinical outcome-a cross-entity comparison of patients with advanced non-small cell lung cancer and colorectal cancer *Oncogene* **38**, 2953-2966 10.1038/s41388-018-0634-0
36. Francis, J. W., Hausmann, S., Ikram, S., Yin, K., Mealey-Farr, R., Flores, N. M. *et al.* (2024) FAM86A methylation of eEF2 links mRNA translation elongation to tumorigenesis *Mol Cell* **84**, 1753-1763 e1757 10.1016/j.molcel.2024.02.037
37. Li, Y., Trojer, P., Xu, C. F., Cheung, P., Kuo, A., Drury, W. J., 3rd *et al.* (2009) The target of the NSD family of histone lysine methyltransferases depends on the nature of the substrate *J Biol Chem* **284**, 34283-34295 M109.034462 [pii]10.1074/jbc.M109.034462
38. Seeliger, D., Soeroes, S., Klingberg, R., Schwarzer, D., Grubmuller, H., and Fischle, W. (2012) Quantitative assessment of protein interaction with methyl-lysine analogues by hybrid computational and experimental approaches *ACS Chem Biol* **7**, 150-154 10.1021/cb200363r
39. Nitsch, S., Zorro Shahidian, L., and Schneider, R. (2021) Histone acylations and chromatin dynamics: concepts, challenges, and links to metabolism *EMBO Rep* **22**, e52774 10.15252/embr.202152774
40. Ghoneim, M., Fuchs, H. A., and Musselman, C. A. (2021) Histone Tail Conformations: A Fuzzy Affair with DNA *Trends Biochem Sci* **46**, 564-578 10.1016/j.tibs.2020.12.012
41. Jain, K., Marunde, M. R., Burg, J. M., Gloor, S. L., Joseph, F. M., Poncha, K. F. *et al.* (2023) An acetylation-mediated chromatin switch governs H3K4 methylation read-write capability *Elife* **12**, 10.7554/eLife.82596
42. Marunde, M. R., Fuchs, H. A., Burg, J. M., Popova, I. K., Vaidya, A., Hall, N. W. *et al.* (2024) Nucleosome conformation dictates the histone code *Elife* **13**, 10.7554/eLife.78866
43. Fox, G. C., Poncha, K. F., Smith, B. R., van der Maas, L. N., Robbins, N. N., Graham, B. *et al.* (2024) Histone H3K18 & H3K23 acetylation directs establishment of MLL-mediated H3K4 methylation *J Biol Chem* **300**, 107527 10.1016/j.jbc.2024.107527

44. Li, W., Tian, W., Yuan, G., Deng, P., Sengupta, D., Cheng, Z. *et al.* (2021) Molecular basis of nucleosomal H3K36 methylation by NSD methyltransferases *Nature* **590**, 498-503 10.1038/s41586-020-03069-8
45. de Napoles, M., Mermoud, J. E., Wakao, R., Tang, Y. A., Endoh, M., Appanah, R. *et al.* (2004) Polycomb group proteins Ring1A/B link ubiquitylation of histone H2A to heritable gene silencing and X inactivation *Dev Cell* **7**, 663-676 10.1016/j.devcel.2004.10.005
46. Bilokapic, S., and Halic, M. (2019) Nucleosome and ubiquitin position Set2 to methylate H3K36 *Nat Commun* **10**, 3795 10.1038/s41467-019-11726-4
47. Luscan, A., Laurendeau, I., Malan, V., Francannet, C., Odent, S., Giuliano, F. *et al.* (2014) Mutations in SETD2 cause a novel overgrowth condition *J Med Genet* **51**, 512-517 10.1136/jmedgenet-2014-102402
48. Lawrence, M. S., Stojanov, P., Mermel, C. H., Robinson, J. T., Garraway, L. A., Golub, T. R. *et al.* (2014) Discovery and saturation analysis of cancer genes across 21 tumour types *Nature* **505**, 495-501 10.1038/nature12912
49. Liu, Y., Zhang, Y., Xue, H., Cao, M., Bai, G., Mu, Z. *et al.* (2021) Cryo-EM structure of SETD2/Set2 methyltransferase bound to a nucleosome containing oncohistone mutations *Cell Discov* **7**, 32 10.1038/s41421-021-00261-6
50. Markert, J. W., Soffers, J. H., and Farnung, L. (2025) Structural basis of H3K36 trimethylation by SETD2 during chromatin transcription *Science* **387**, 528-533 10.1126/science.adn6319
51. Hacker, K. E., Fahey, C. C., Shinsky, S. A., Chiang, Y. J., DiFiore, J. V., Jha, D. K. *et al.* (2016) Structure/Function Analysis of Recurrent Mutations in SETD2 Protein Reveals a Critical and Conserved Role for a SET Domain Residue in Maintaining Protein Stability and Histone H3 Lys-36 Trimethylation *J Biol Chem* **291**, 21283-21295 10.1074/jbc.M116.739375
52. Wang, Z., Hausmann, S., Lyu, R., Li, T. M., Lofgren, S. M., Flores, N. M. *et al.* (2020) SETD5-Coordinated Chromatin Reprogramming Regulates Adaptive Resistance to Targeted Pancreatic Cancer Therapy *Cancer Cell* **37**, 834-849 e813 10.1016/j.ccell.2020.04.014
53. Jonkers, J., Meuwissen, R., van der Gulden, H., Peterse, H., van der Valk, M., and Berns, A. (2001) Synergistic tumor suppressor activity of BRCA2 and p53 in a conditional mouse model for breast cancer *Nat Genet* **29**, 418-425 10.1038/ng747
54. Raymond, C. S., and Soriano, P. (2007) High-efficiency FLP and PhiC31 site-specific recombination in mammalian cells *PloS one* **2**, e162 10.1371/journal.pone.0000162
55. Liu, S., Hausmann, S., Carlson, S. M., Fuentes, M. E., Francis, J. W., Pillai, R. *et al.* (2019) METTL13 Methylation of eEF1A Increases Translational Output to Promote Tumorigenesis *Cell* **176**, 491-504 e421 10.1016/j.cell.2018.11.038
56. Park, J., Wu, J., Szkop, K. J., Jeong, J., Jovanovic, P., Husmann, D. *et al.* (2024) SMYD5 methylation of rpL40 links ribosomal output to gastric cancer *Nature* 10.1038/s41586-024-07718-0

FIGURE LEGENDS

Fig 1. SETD2 ablation promotes KRAS^{G12C}-driven lung tumorigenesis in vivo.

A, Schematic of the *Setd2$^{LoxP/LoxP}$* conditional allele. In the presence of Cre recombinase, exon 3 is deleted to disrupt *Setd2* expression. **B,** Confirmation of *Setd2$^{LoxP/LoxP}$* conditional allele by PCR on DNA isolated from mouse tail biopsies from indicated mouse genotypes, expected product sizes are marked. C, Schematic of generation of LUAD model driven by Cre-recombinase inducible conditional oncogenic *Kras^{G12C}* mutation and deletion of p53 (*K^{C}P*) and *Setd2* (*K^{C}P;Setd2*). **D,** Experimental design to assess effects of SETD2 ablation on LUAD pathogenesis in *K^{C}P* model. **E,** Representative HE and IHC staining with indicated antibodies of lung tumors from *K^{C}P* and *K^{C}P;Setd2* mutant mice at 10 weeks after Ad-Cre induction (n=6/group). H3K36me3 serves as a proxy of SETD2 ablation in tumor cells in *K^{C}P;Setd2* mutant mice. P values determined by two-tailed unpaired t-test; boxes: 25th to 75th percentile, whiskers: min. to max., center line: median; scale bars: 100 µm. **F-I,** Quantification of tumor number, tumor burden, proliferation (Ki67+) and cell death (cleaved Caspase3+) in *K^{C}P* and *K^{C}P;Setd2* samples as in e. **J,** Kaplan-Meier survival curves of *K^{C}P* control (n=8, median survival 151 days) and *K^{C}P;Setd2* mutant mice (n=8, median survival 92 days) mutant mice. *P* values determined by the log-rank test.

Fig 2. SETD2 methylates unmodified, H3K36me1-, and H3K36me2-modified nucleosomes, but not those bearing H3K36me3

A, Schematic of SETD2 domain structure, with the catalytic region used in the biochemical assays ($SETD2_{SET}$) indicated. **B,** $SETD2_{SET}$ *in vitro* methylation reactions with radiolabeled ^{3}H-SAM on unmodified (H3), H3K36me1, H3K36me2, or H3K36me3 recombinant nucleosomes (rNuc) substrates as indicated. K36me: methylated H3K36. Top, autoradiography; bottom, Coomassie blue staining. **C,** Methylation (MTase-Glo) assays (see methods) with enzyme and substrates as in (B). SAH concentration serves as a measurement of methylation. Activity is normalized to control conditions. Data are means ± SEM from 3 independent replicates. *P* values determined by one-way ANOVA. **D,** Methylation reactions as in (B) using $NSD2_{SET}$ as the enzyme and the indicated rNucs as substrates. Top, autoradiography; bottom, Coomassie blue staining. **E,** Western blot analysis with the indicated antibodies on the indicated rNucs as in (B). **F,** $SETD2_{SET}$ methylation assays as in (B) using non-radiolabeled SAM and methylation detected by Western analyses using the antibodies characterized in (E). H3 is shown as a loading control.

Fig 3. Histone poly-acetylation enhances SETD2$_{SET}$ activity

A, Schematic showing the tetra-acetylated rNuc tested in the study. **B,** *In vitro* methylation reactions with SETD2$_{SET}$ as in Fig. 2B using the indicated tetra-acetylated rNucs. Top, autoradiography; bottom, Coomassie blue staining. **C,** MTase-Glo assays as in Fig. 2C using the indicated tetra-acetylated rNucs. Data are means ± SEM from 12 independent replicates. *P* values determined by one-way ANOVA. **D,** Methylation reactions as in (B) using NSD2$_{SET}$ as enzyme. Top, autoradiography; bottom, Coomassie blue staining. **E,** Methylation reactions as in (B) using DOT1L as enzyme. Top, autoradiography; bottom, Coomassie blue staining.

Fig 4. H3K27 acetylation enhances SETD2$_{SET}$ binding and activity

A, Schematic showing the different histone H3 acetylated rNuc tested in the study. **B,** *In vitro* methylation reactions with SETD2$_{SET}$ as in Fig. 2B using the indicated acetylated rNucs. Top, autoradiography; bottom, Coomassie blue staining. **C,** MTase-Glo assays as in Fig. 2C using the indicated acetylated rNucs. Data are means ± SEM from 6 independent replicates. *P* values determined by one-way ANOVA. **D,** Nucleosome pulldown assay using biotinylated unmodified or H3K27ac nucleosomes as bait to assess binding to GST-SETD2$_{SET}$. Bound protein was detected by Western blotting with indicated antibodies. **E,** Electrophoretic mobility shift assay (EMSA) with increasing concentrations of SETD2$_{SET}$ (0–5 μM) incubated with the indicated rNuc (250 nM) and SETD2$_{SET}$ binding to rNuc detected by staining DNA with Sybr Gold.

Fig 5. Histone ubiquitination does not affect SETD2$_{SET}$ activity

A, Schematic showing the different histone ubiquitinated rNuc tested in the study. **B,** *In vitro* methylation reactions with SETD2$_{SET}$ as in Figure 2B using the indicated ubiquitinated rNucs. Top, autoradiography; bottom, Coomassie blue staining. **C,** SETD2$_{SET}$ methylation assays as in Fig. 2F using non-radiolabeled SAM and methylation detected by Western analysis using the indicated antibodies. H3 is shown as a loading control. Note that H3K14ub and H3K18ub interfere with the αH3K36me2 antibody from recognizing H3K36me2. **D,** MTase-Glo assays as in Fig. 2C using the indicated rNucs. Data are means ± SEM from 6 independent replicates. *P* values determined by one-way ANOVA. **E,** Methylation reactions as in (B) using NSD2$_{SET}$ as enzyme. Top, autoradiography; bottom, Coomassie blue staining.

Author Contributions

R.J.M. and N.M.F. contributed equally to this work. They were responsible for experimental design, execution, data analysis, and manuscript preparation for their sections of the work. G.C.F. contributed to analysis of histone acetylation on SETD2 activity and nucleosome binding under the supervision of J.M.D. and B.D.S. H.D. and M.C. helped R.J.M. perform NSD2 assays. S.H. and T.C. contributed to histopathological evaluation and IHC analysis. O.G. and P.K.M. were equally responsible for supervision of research, data interpretation and manuscript preparation.

Competing Interests

O.G. is a co-scientific founder and shareholders of K36 Therapeutics, Inc. and Alternative Bio, Inc. P.K.M. is a consultant and stockholder of Ikena Oncology, Inc. and Alternative bio, Inc. O.G. and B.D.S. are board members, co-scientific founders, and shareholders of EpiCypher, Inc. The other authors declare no competing interests.

DATA AVAILABILITY

Plasmids, antibodies, and cell lines generated in this study will be available from the lead contact upon request with a completed material transfer agreement.

Figure 1

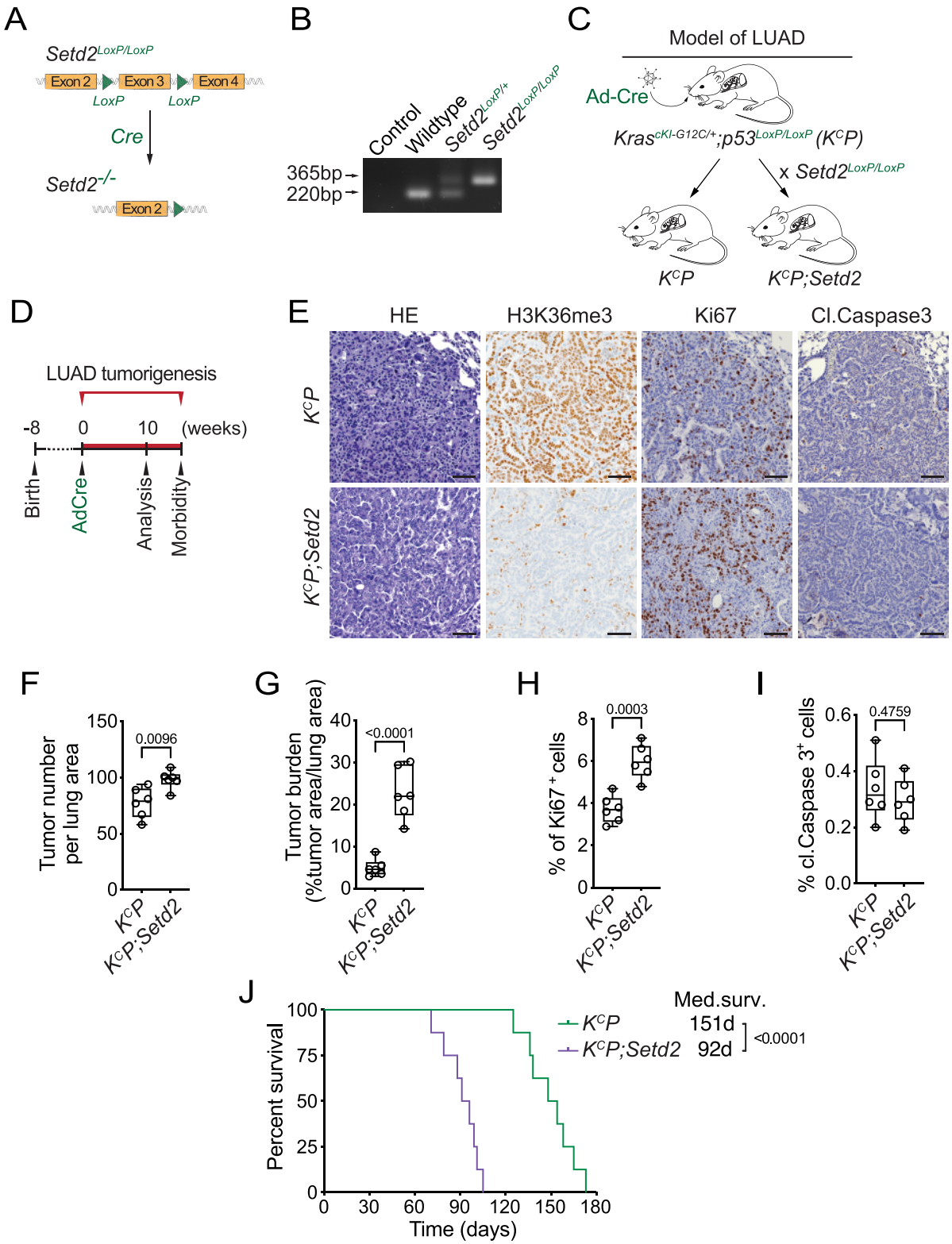
A
Setd2LoxP/LoxP
Exon 2
Exon 3
Exon 4
LoxP
LoxP
Cre
Setd2-/-
Exon 2
B
Control
Wildtype
Setd2LoxP/+
Setd2LoxP/LoxP
365bp
220bp
C
Model of LUAD
Ad-Cre
KrascKI-G12C/+;p53LoxP/LoxP (KCP)
x Setd2LoxP/LoxP
KCP
KCP;Setd2
D
LUAD tumorigenesis
-8
0
10
(weeks)
Birth
AdCre
Analysis
Morbidity
E
HE
H3K36me3
Ki67
Cl.Caspase3
KCP
KCP;Setd2
F
Tumor number per lung area
0.0096
KCP
KCP;Setd2
G
Tumor burden (%tumor area/lung area)
<0.0001
KCP
KCP;Setd2
H
% of Ki67+ cells
0.0003
KCP
KCP;Setd2
I
% cl.Caspase 3+ cells
0.4759
KCP
KCP;Setd2
J
Percent survival
Time (days)
KCP
KCP;Setd2
Med.surv.
151d
92d
<0.0001

Figure 2

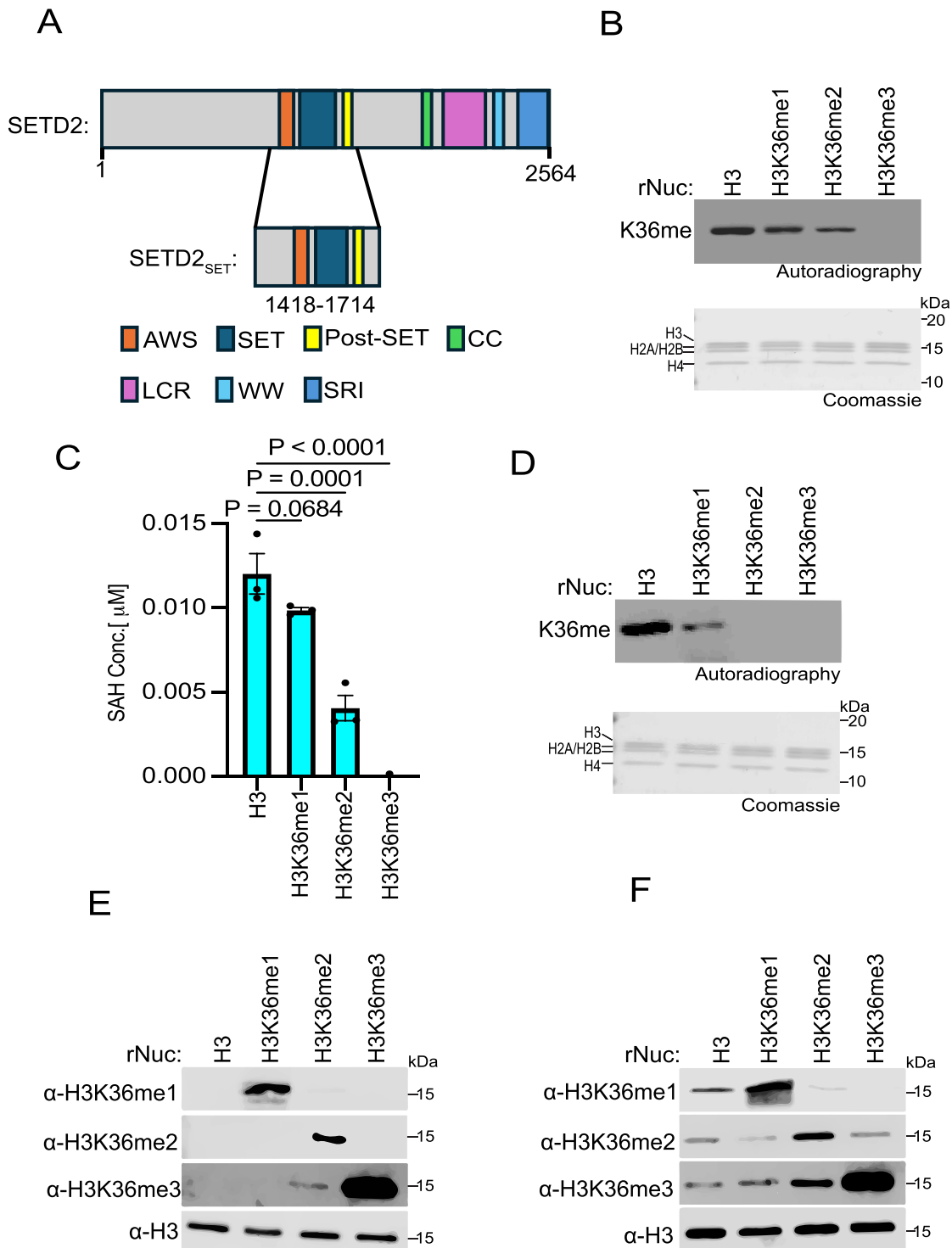
A
SETD2:
1
2564
SETD2SET:
1418-1714
AWS
SET
Post-SET
CC
LCR
WW
SRI
B
rNuc:
H3
H3K36me1
H3K36me2
H3K36me3
K36me
Autoradiography
kDa
20
15
10
H3
H2A/H2B
H4
Coomassie
C
P < 0.0001
P = 0.0001
P = 0.0684
SAH Conc.[μM]
0.015
0.010
0.005
0.000
H3
H3K36me1
H3K36me2
H3K36me3
D
rNuc:
H3
H3K36me1
H3K36me2
H3K36me3
K36me
Autoradiography
kDa
20
15
10
H3
H2A/H2B
H4
Coomassie
E
rNuc:
H3
H3K36me1
H3K36me2
H3K36me3
kDa
α-H3K36me1
α-H3K36me2
α-H3K36me3
α-H3
15
F
rNuc:
H3
H3K36me1
H3K36me2
H3K36me3
kDa
α-H3K36me1
α-H3K36me2
α-H3K36me3
α-H3
15

Figure 3

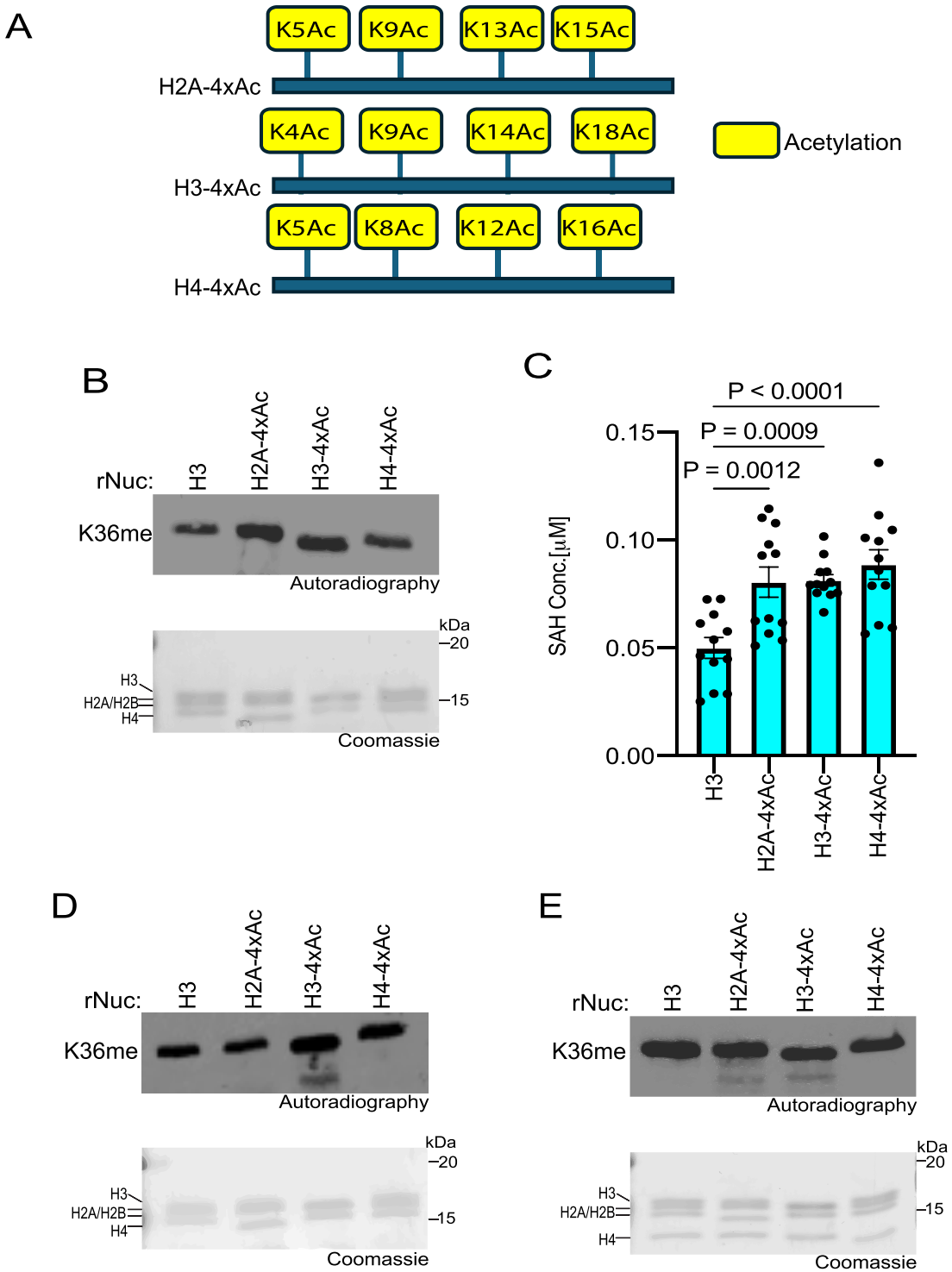
A
K5Ac
K9Ac
K13Ac
K15Ac
H2A-4xAc
K4Ac
K9Ac
K14Ac
K18Ac
H3-4xAc
K5Ac
K8Ac
K12Ac
K16Ac
H4-4xAc
Acetylation
B
rNuc:
H3
H2A-4xAc
H3-4xAc
H4-4xAc
K36me
Autoradiography
kDa
20
15
H3
H2A/H2B
H4
Coomassie
C
P < 0.0001
P = 0.0009
P = 0.0012
SAH Conc.[μM]
0.15
0.10
0.05
0.00
H3
H2A-4xAc
H3-4xAc
H4-4xAc
D
rNuc:
H3
H2A-4xAc
H3-4xAc
H4-4xAc
K36me
Autoradiography
kDa
20
15
H3
H2A/H2B
H4
Coomassie
E
rNuc:
H3
H2A-4xAc
H3-4xAc
H4-4xAc
K36me
Autoradiography
kDa
20
15
H3
H2A/H2B
H4
Coomassie

Figure 4

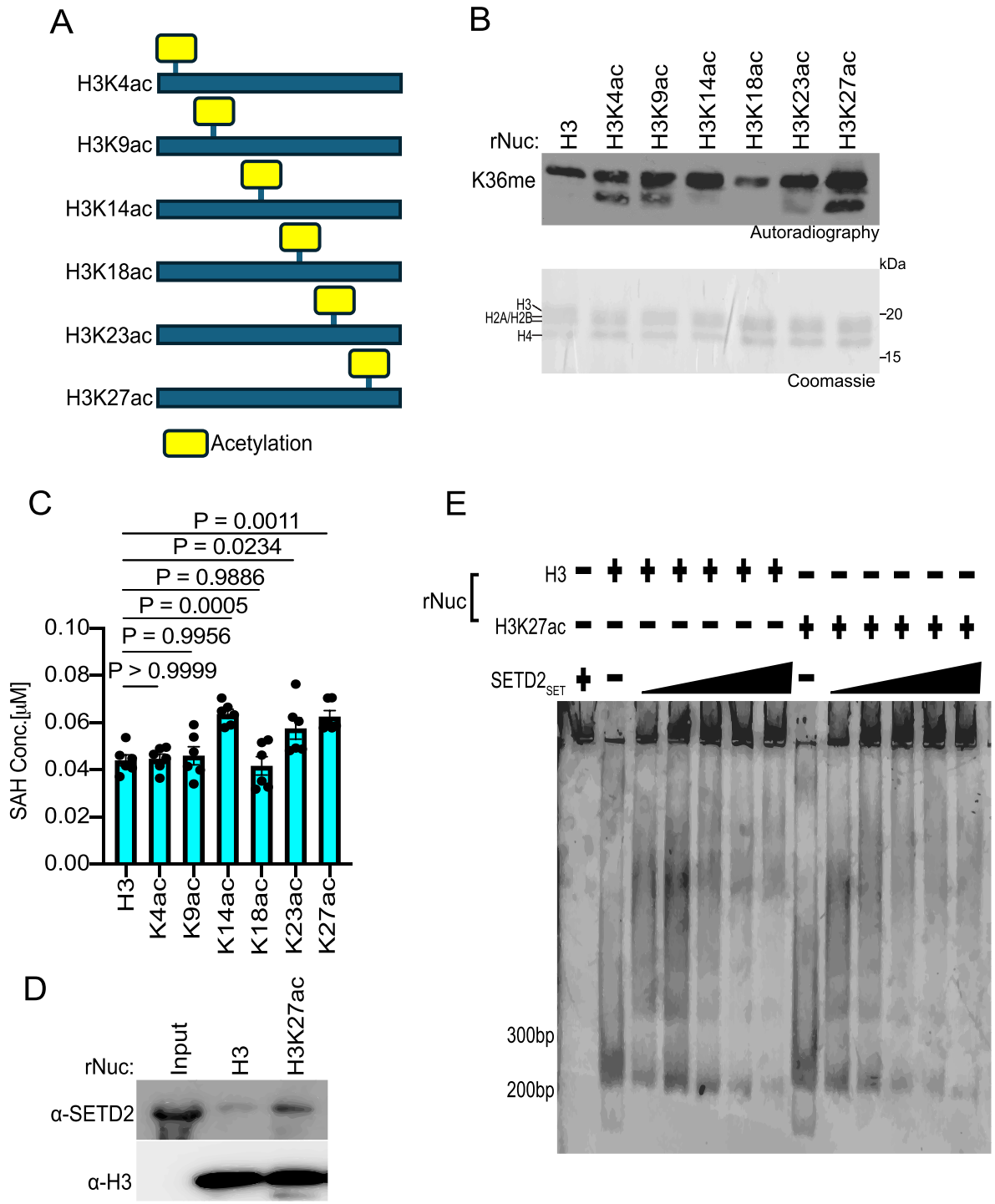
A
H3K4ac
H3K9ac
H3K14ac
H3K18ac
H3K23ac
H3K27ac
Acetylation
B
rNuc:
H3
H3K4ac
H3K9ac
H3K14ac
H3K18ac
H3K23ac
H3K27ac
K36me
Autoradiography
kDa
H3
H2A/H2B
H4
20
15
Coomassie
C
P = 0.0011
P = 0.0234
P = 0.9886
P = 0.0005
P = 0.9956
P > 0.9999
SAH Conc.[μM]
0.10
0.08
0.06
0.04
0.02
0.00
H3
K4ac
K9ac
K14ac
K18ac
K23ac
K27ac
D
rNuc:
Input
H3
H3K27ac
α-SETD2
α-H3
E
rNuc
H3
H3K27ac
SETD2SET
300bp
200bp

Figure 5

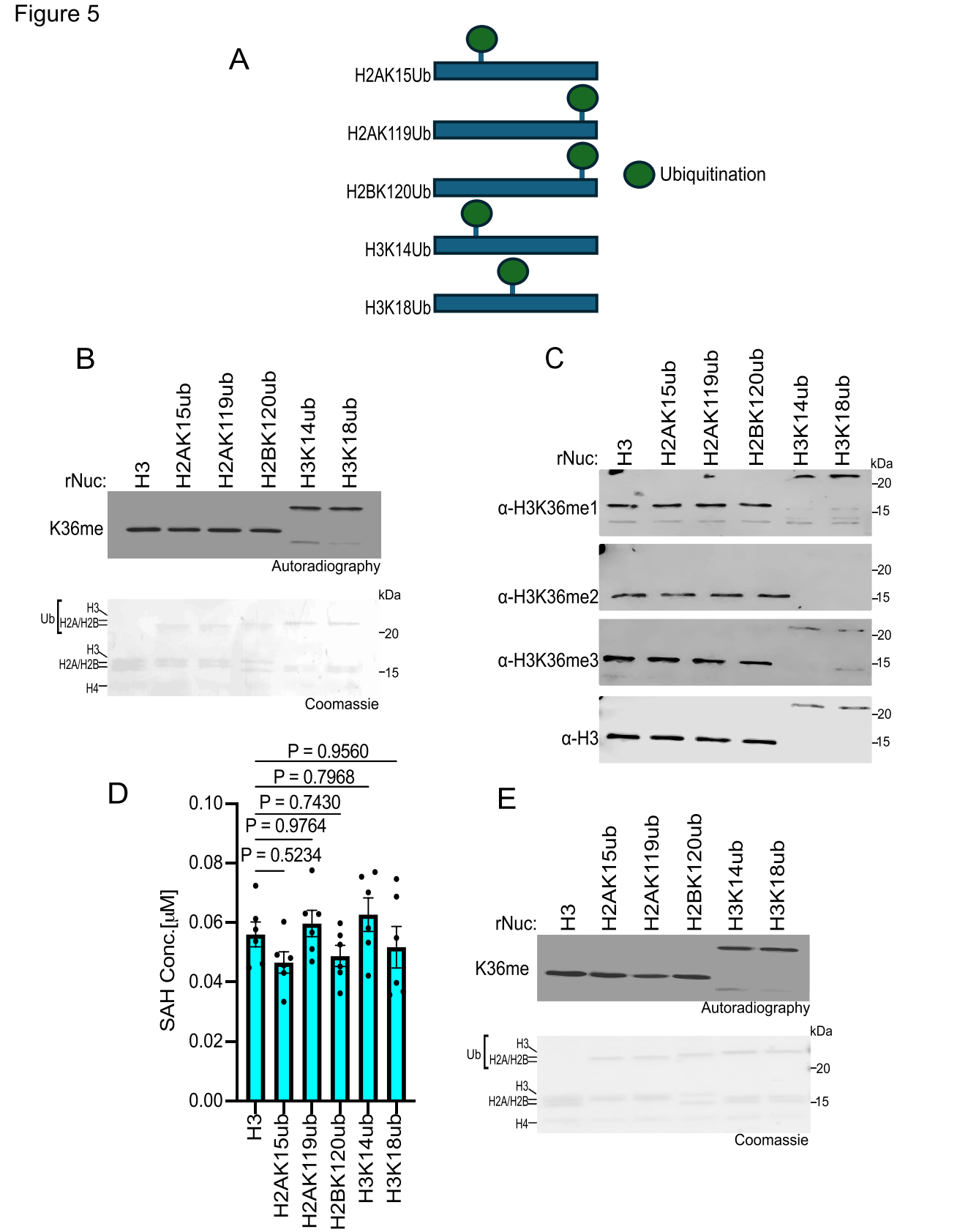
A
H2AK15Ub
H2AK119Ub
H2BK120Ub
H3K14Ub
H3K18Ub
Ubiquitination
B
rNuc:
H3
H2AK15ub
H2AK119ub
H2BK120ub
H3K14ub
H3K18ub
K36me
Autoradiography
kDa
Ub
H3
H2A/H2B
H4
20
15
Coomassie
C
rNuc:
H3
H2AK15ub
H2AK119ub
H2BK120ub
H3K14ub
H3K18ub
kDa
α-H3K36me1
α-H3K36me2
α-H3K36me3
α-H3
20
15
D
P = 0.9560
P = 0.7968
P = 0.7430
P = 0.9764
P = 0.5234
SAH Conc.[μM]
0.10
0.08
0.06
0.04
0.02
0.00
H3
H2AK15ub
H2AK119ub
H2BK120ub
H3K14ub
H3K18ub
E
rNuc:
H3
H2AK15ub
H2AK119ub
H2BK120ub
H3K14ub
H3K18ub
K36me
Autoradiography
kDa
Ub
H3
H2A/H2B
H4
20
15
Coomassie